

K_V10.1 opposes activity-dependent increase in Ca²⁺ influx into the presynaptic terminal of the parallel fibre–Purkinje cell synapse

Lena Sünke Mortensen^{1,2}, Hartmut Schmidt³, Zohreh Farsi¹, Alonso Barrantes-Freer¹, María E. Rubio¹, Roser Ufartes¹, Jens Eilers³, Takeshi Sakaba⁴, Walter Stühmer^{1,5} and Luis A. Pardo¹

¹Max-Planck-Institute of Experimental Medicine, 37075 Göttingen, Germany

²International Max Planck Research School Neurosciences, 37077 Göttingen, Germany

³Carl-Ludwig-Institute of Physiology, 04103 Leipzig, Germany

⁴Max-Planck-Institute of Biophysical Chemistry, 37077 Göttingen, Germany

⁵Center for Molecular Physiology of the Brain (CMPB), 37077 Göttingen, Germany

Key points

- Voltage-gated K_V10.1 potassium channels are widely expressed in the mammalian brain but their function remains poorly understood.
- We report that K_V10.1 is enriched in the presynaptic terminals and does not take part in somatic action potentials.
- In parallel fibre synapses in the cerebellar cortex, we find that K_V10.1 regulates Ca²⁺ influx and neurotransmitter release during repetitive high-frequency activity.
- Our results describe the physiological role of mammalian K_V10.1 for the first time and help understand the fine-tuning of synaptic transmission.

Abstract The voltage-gated potassium channel K_V10.1 (Eag1) is widely expressed in the mammalian brain, but its physiological function is not yet understood. Previous studies revealed highest expression levels in hippocampus and cerebellum and suggested a synaptic localization of the channel. The distinct activation kinetics of K_V10.1 indicate a role during repetitive activity of the cell. Here, we confirm the synaptic localization of K_V10.1 both biochemically and functionally and that the channel is sufficiently fast at physiological temperature to take part in repolarization of the action potential (AP). We studied the role of the channel in cerebellar physiology using patch clamp and two-photon Ca²⁺ imaging in K_V10.1-deficient and wild-type mice. The excitability and action potential waveform recorded at granule cell somata was unchanged, while Ca²⁺ influx into axonal boutons was enhanced in mutants in response to stimulation with three APs, but not after a single AP. Furthermore, mutants exhibited a frequency-dependent increase in facilitation at the parallel fibre–Purkinje cell synapse at high firing rates. We propose that K_V10.1 acts as a modulator of local AP shape specifically during high-frequency burst firing when other potassium channels suffer cumulative inactivation.

(Resubmitted 28 July 2014; accepted after revision 13 October 2014; first published online 24 October 2014)

Corresponding author Luis A. Pardo: Max-Planck-Institute of Experimental Medicine, Hermann-Rein-Str. 3, 37075 Göttingen, Germany. Email: pardo@em.mpg.de

Abbreviations AP, action potential; Ca_{res}, residual calcium; GC, granule cell; HVA, high voltage activating; LVA, low voltage activating; (m)EPSC, (miniature) excitatory postsynaptic current; OGB, Oregon Green BAPTA-1; PC, Purkinje cell; PF, parallel fibre; *p_r*, release probability; RRP, readily releasable pool; TBST, Tris-buffered saline–Tween 20.

Introduction

Neuronal potassium channels are involved in setting the resting membrane potential, influencing firing patterns, repolarizing the action potential (AP), and in controlling neurotransmitter release and synaptic plasticity. $K_V10.1$ is the founding member of the *eag* (*ether-à-go-go*) family of voltage-gated potassium channels (Warmke & Ganetzky, 1994). In mammals, channel expression is restricted to the CNS (Ludwig *et al.* 1994; Saganich *et al.* 2001; Martin *et al.* 2008). While *Drosophila eag* is implicated in controlling neuronal excitability (Wu *et al.* 1983), little is known about the physiological role of $K_V10.1$ in higher organisms. A biophysical hallmark of $K_V10.1$ is that it activates orders of magnitude faster at depolarized potentials than at hyperpolarized potentials (Ludwig *et al.* 1994); this provides the channel with a short-term molecular memory and could make its role dependent on the average potential previous to the AP and therefore on activity. Electron microscopy, single particle tracking (Gómez-Varela *et al.* 2010), and recent immunocytochemistry and biochemical data (Chuang *et al.* 2014) indicate a (pre)synaptic localization of $K_V10.1$. As no specific pharmacological blockers for $K_V10.1$ are available, $K_V10.1$ -deficient mice represent the best possibility to analyse its significance in neuronal function. $K_V10.1$ knock-out (KO) mice are viable and show no obvious abnormal behaviour except increased spontaneous locomotor activity (Ufartes *et al.* 2013). We compared the synaptic transmission at the parallel fibre–Purkinje cell (PF–PC) synapse of wild-type (WT) and $K_V10.1$ KO mice to study the physiological role of $K_V10.1$. The PF–PC synapse has a moderate release probability (p_r) (Dittman *et al.* 2000; Isope & Barbour, 2002; Sims & Hartell, 2005; Valera *et al.* 2012; Schmidt *et al.* 2013) and exhibits paired-pulse facilitation (Konnerth *et al.* 1990) that can be caused by several mechanisms including residual free Ca^{2+} (Ca_{res}), a facilitated release machinery, or buffer saturation (reviewed by Zucker and Regehr, 2002). In hippocampal mossy fibre boutons (Wheeler *et al.* 1996; Geiger & Jonas, 2000) and in the calyx of Held (Borst & Sakmann, 1999; Ishikawa *et al.* 2003), it has been shown that the width of an AP determines the duration of the Ca^{2+} nanodomain signal that triggers release (Bollmann & Sakmann, 2005) and subsequently influences synaptic plasticity. We found that single excitatory postsynaptic currents (EPSCs) recorded from Purkinje cells are unchanged in $K_V10.1$ KO mice, but that they are differently affected by changes in the extracellular Ca^{2+} concentrations. By two-photon Ca^{2+} imaging we show that loss of $K_V10.1$ causes a frequency- and pulse number-dependent increase in presynaptic Ca^{2+} signals. Additionally, facilitation is increased in $K_V10.1$ KO mice at the PF–PC synapses. Somatic excitability of granule cells (GCs) is unchanged in $K_V10.1$ KO mice, suggesting that the phenotype originates at the synapse.

Our results suggest that $K_V10.1$ is important for regulating AP width at high-frequency stimulus trains and thereby contributes to regulating synaptic strength.

Methods

Ethical statement

All experiments were done following the guidelines of the German law on animal protection.

HEK cell electrophysiology

Monoclonal HEK293 cells expressing hEag1 (García-Ferreiro *et al.* 2004) were grown for 24–72 h on poly-L-lysine-coated glass coverslips. Macroscopic currents were recorded in the whole-cell configuration of the patch-clamp technique using an EPC-9 amplifier and Pulse software (HEKA, Lambrecht/Pfalz, Germany). Patch pipettes with a tip resistance of 1.5–2 M Ω were made from Corning no. 0010 capillary glass (World Precision Instruments, Sarasota, FL, USA). The internal solution contained (in mM) 100 KCl, 45 *N*-methyl-D-glucamine, 10 BAPTA.K₄ and 10 Hepes/HCl (pH 7.35). The control external recording solution contained (in mM) 160 NaCl, 2.5 KCl, 2 CaCl₂, 1 MgCl₂, 8 glucose and 10 Hepes/NaOH (pH 7.4). Series resistance was determined using the automated capacity compensation of the amplifier and compensated for by 60–80%. Currents were elicited by injection of square voltage pulses, sampled at 20 kHz and filtered at 4 kHz. To determine the *I*–*V* relationship, cells were held at –60 mV and voltage pulses ranging from –60 to +80 mV were injected. To determine the dependence of activation kinetics on the prepulse potential, cells were stepped to +40 mV from a 5 s prepulse ranging from –120 to –70 mV and the rise time between 10 and 80% of the maximal current calculated. The Q_{10} value was calculated as

$$Q_{10} = \left(\frac{R_2}{R_1} \right)^{10/(T_2 - T_1)}$$

with R_2 and R_1 being the rise times, and T_2 and T_1 the temperature.

Data analysis was performed offline with PulseFit software (HEKA).

Slice preparation and electrophysiology

Slices were prepared as described previously (Bao *et al.* 2010). Briefly, $K_V10.1$ KO mice and WT littermates (postnatal day (P)20–28) were decapitated under isoflurane (Essex Tierarznei, Munich, Germany) anaesthesia. The cerebellum was removed and placed in an ice-cold oxygenated solution containing (in mM) 60 NaCl, 120

sucrose, 25 NaHCO₃, 1.25 NaH₂PO₄, 2.5 KCl, 25 D-glucose, 0.1 CaCl₂, 3 MgCl₂, 3 *myo*-inositol, 2 sodium pyruvate and 0.4 ascorbic acid. Coronal slices (200 μm) of the cerebellar vermis were cut using a vibratome (VT1200S; Leica, Wetzlar, Germany). The slices were kept at 36°C for 45 min to 1 h in oxygenated artificial cerebrospinal fluid containing (in mM) 125 NaCl, 2.5 KCl, 25 NaHCO₃, 1.25 NaH₂PO₄, 2 CaCl₂, 1 MgCl₂, 3 *myo*-inositol, 2 sodium pyruvate and 0.4 ascorbic acid.

Cells were visually identified and patched at 33 ± 1°C in oxygenated artificial cerebrospinal fluid using an EPC 10/2 amplifier controlled by Patchmaster software (HEKA). Thick-walled borosilicate pipettes were pulled to resistances of 3–4 MΩ for Purkinje cell recordings and 6–7 MΩ for granule cells when filled with intracellular solution containing (in mM) 135 potassium gluconate, 5 KCl, 10 Hepes, 5 MgATP, 0.5 NaGTP, 1 EGTA and 5 *N*-(2,6-dimethylphenylcarbamoylmethyl)-triethylammonium chloride (QX-314; Tocris, Ellisville, MO, USA; a Na⁺ channel blocker to prevent clamp escape). Liquid junction potential was assumed to be 10 mV; the reported voltages were not corrected for liquid junction potential. For recording of evoked EPSCs, voltage pulses (20 μs, 1–5 V) were applied through an extracellular electrode placed in the GC layer and the GABA_A receptor antagonist 2-(3-carboxypropyl)-3-amino-6-(4-methoxyphenyl)pyridazinium bromide (SR-95531; Tocris) was added. Series resistance was compensated for to leave ≤ 5 MΩ uncompensated resistance. QX-314 was omitted in current clamp recordings. Extracellular potentials were recorded in the molecular layer while voltage pulses were applied through an electrode placed 200–600 μm lateral to the recording site. Spontaneous miniature (m)EPSCs were recorded in Purkinje cells in sagittal slices in the presence of 1 μM TTX (Alomone, Jerusalem, Israel) and 100 μM picrotoxin (Tocris).

Data acquisition and analysis

Data were low-pass filtered at 5–10 kHz and sampled at 50–100 kHz. Offline analysis was performed with custom-written macros in Igor Pro (Wavemetrics, Lake Oswego, OR, USA). Trains of EPSCs were recorded 10–20 times and averaged per cell. Statistical analysis was performed with Prism software (GraphPad Software Inc., La Jolla, CA, USA). All data are presented as mean ± SEM and Student's *t* test was used to test for statistical significance if not noted otherwise.

Variance mean analysis

Variance mean analysis for determination of synaptic parameters is an established tool for analysis of synaptic parameters (Silver *et al.* 1998; Reid & Clements, 1999;

Clements & Silver, 2000; Humeau *et al.* 2001, 2002, 2007; Silver, 2003). It has been employed in experimental paradigms using extracellular stimulation at the PF–PC synapse previously (Sims & Hartell, 2005; Valera *et al.* 2012). Briefly, the binomial model of release describes the mean of the response

$$I_{\text{mean}} = N \cdot p_r \cdot Q$$

with *N* being a binomial parameter that can reflect the number of independent release sites under certain conditions (Meyer *et al.* 2001) with average release probability *p_r* and quantal size *Q*. The variance of the response is given by

$$\text{Var}_I = N \cdot p_r \cdot (1 - p_r) \cdot Q^2.$$

Modifying *p_r* by changing the concentration of extracellular Ca²⁺, $\text{Var}_I = f(I_{\text{mean}})$ takes the form of a parabola:

$$\text{Var}_I = Q \cdot I_{\text{mean}} - \frac{I_{\text{mean}}^2}{N} \quad (1)$$

where the initial slope of the parabola provides an estimate for *Q* and the greater *x*-axis intercept of the parabola for (*N* · *Q*). *p_r* can be estimated from the parabola, as it will be 0.5 at the peak and 1 at the greater *x*-axis intercept. This model greatly simplifies the physiological situation, as it assumes uniformity of *p_r* and *Q* across release sites and linear summation of individual quantal responses. Furthermore, *N* is merely a functional parameter, representing the number of release sites with release-ready vesicles at the time of stimulation, and excluding silent sites (Humeau *et al.* 2007; Valera *et al.* 2012).

In each cell, we recorded ≥ 50 EPSCs in 2, 4, 0.5 and again 2 mM Ca²⁺. Cells were only used for analysis if series resistance changed less than 10% during recording and if the average EPSC amplitude in the initial and final records in 2 mM Ca²⁺ did not differ. Variances of the average EPSC amplitudes under the different recording conditions were plotted against the respective means and fitted with eq. (1). To compare data from WT and K_V10.1 KO cells, the data were normalized to the maximum variance and *x*-axis intercept of the parabolas.

Two-photon-Ca²⁺ imaging in axonal boutons

GCs were whole-cell patch-clamped and filled via the pipette with intracellular solution containing 0.1 mM Oregon Green 488 BAPTA-1 (OGB; Invitrogen, Carlsbad, CA, USA). The axon was visually identified and presumed synaptic boutons were visible as varicosities along the axon. For analysis, preference was given to boutons that were found distally to the bifurcation of the axon (see also Fig. 5). Current pulses of 1 ms duration were given to elicit

1–3 APs at 50–100 Hz 30–60 min after breaking into the cell. Fluorescence signals in the boutons were recorded at 33°C by performing a line scan across the bouton with a laser-scanning microscope (Olympus). Offline analysis was performed in Fluoview (Olympus) and Igor Pro with custom-written algorithms. Background fluorescence was corrected for and the change in intensity was divided by the baseline fluorescence resulting in $\Delta F/F_0$ values. After manual identification of a maximum, the signal decay was fitted with an exponential function. The amplitude parameter of the fit was used for statistical analysis.

Subcellular fractioning and Western blotting

Synaptosomes were prepared as previously described (Fischer von Mollard *et al.* 1991). Briefly, 4-week-old mice (K_V10.1 KO and WT littermates) were decapitated and their brains were removed. After homogenization in ice-cold homogenization buffer (320 mM sucrose, 5 mM Hepes, pH 7.4), cell debris was removed by centrifugation at 3000 g for 2 min at 4°C. Synaptosomes were then collected by re-centrifuging the supernatant for 12 min at 14,000 g, and laid on a three-step discontinuous Ficoll gradient consisting of 4 ml 13% Ficoll, 1 ml 9% Ficoll and 4 ml 6% Ficoll. After centrifugation of the gradients at 75,000 g for 35 min, the synaptosome band at the interface between 13% and 9% Ficoll was collected, diluted in homogenization buffer and again centrifuged for 12 min at 14,000 g to remove Ficoll. The isolated synaptosomes (5 mg) were resuspended in 20 ml sucrose buffer (320 mM sucrose, 5 mM Hepes, pH 8) and supplemented with 50 μ g trypsin (Roche, Indianapolis, IN, USA) to give a final protein/protease ratio of 100:1. Proteolytic digestion of the post-synaptic membranes was performed by incubation of synaptosomes with the protease for 30 min at 30°C. Afterwards, the synaptosomes were pelleted by centrifugation at 22,500 r.p.m. in a Beckman SW41 swing-out rotor for 35 min and protease activity was blocked by addition of Pefabloc (Roche). Samples were separated by SDS-PAGE and proteins were subsequently transferred to a nitrocellulose membrane. The membrane was dried for 30 min at 37°C for Western blotting. After rehydration, the Quentix Western Blot Enhancer (Pierce, Rockford, IL, USA) was applied, the membrane was washed in H₂O and incubated in 5% non-fat milk in Tris-buffered saline–Tween 20 (TBST) before application of primary antibodies against K_V10.1 (Chen *et al.* 2011), AMPAR (Synaptic Systems, Göttingen, Germany), synaptophysin (Synaptic Systems) and synaptobrevin 2 (Synaptic Systems). After further washes with TBST, the membrane was incubated with horseradish peroxidase-coupled secondary antibodies for 1 h. The blot was developed using WesternLightening TMPlus-ECL (Perkin Elmer, Waltham, MA, USA) and

protein bands were detected by a luminescence detector (Boehringer Mannheim, Mannheim Germany).

Freeze substitution and post-embedding immunogold labelling

Sprague-Dawley rats were transcardially perfused with 4% paraformaldehyde and 0.5% glutaraldehyde in 0.1 M phosphate buffer, pH 7.15, for 1.5 h. Cerebellar regions were carefully dissected and processed for freeze substitution and low-temperature embedding as previously described (Douyard *et al.* 2007). For post-embedding immunocytochemistry, ultrathin sections (80 nm in thickness) on nickel grids were incubated in sodium borohydride and glycine in TBS solution with Triton X-100. After being preblocked with serum, the sections were incubated with affinity-purified primary antibody mAb62 (1 μ g ml⁻¹; 1:200 dilution). Primary antibody was detected with secondary antibodies conjugated to 5 nm gold particles (1:20; Amersham, Arlington Heights, IL, USA). The specificity of the antibody had been previously confirmed (Hemmerlein *et al.* 2006; Martin *et al.* 2008; Gómez-Varela *et al.* 2010). Controls included omitting mAb62 and preabsorption of mAb62 with the corresponding blocking protein (10 μ g ml⁻¹ final concentration). Ultrathin sections were counterstained with uranyl acetate and lead citrate and studied with a transmission electron microscope. Electron micrographs were taken at 30,000 \times magnification and scanned at a resolution of 3600 d.p.i. using a Linotype-Hell scanner (Heidelberg, Germany). Image processing was performed with Adobe Photoshop using only the brightness and contrast commands to enhance gold particles.

Results

K_V10.1 activation kinetics at near physiological temperature

To date, all available studies on K_V10.1 have been performed at room temperature and report a slow activation of the channel (e.g. Ludwig *et al.* 1994; Terlau *et al.* 1996). When we compared channel properties measured in stably transfected HEK-293 cells at room temperature (25 \pm 1°C) and near physiological temperatures (30 \pm 1°C), we found markedly accelerated activation kinetics (Fig. 1A, B; Q₁₀ of approximately 1.4 at –90 mV holding potential), while the channel conductance remained unchanged (Fig. 1C). Interestingly, upon repeated brief depolarization, the amplitude of the current increased with each pulse (Fig. 1D). This suggests that due to the previously described two activity states of the channel (Ludwig *et al.* 1994; Terlau *et al.* 1996) it switches from a slow state at resting potential to a

'fast mode' during cell activity. This endows the channel with a short-lasting memory of the recent activity of the cell.

Granule cell firing is unaffected in K_V10.1 KO mice

In situ hybridization data suggest expression of K_V10.1 in cerebellar GCs (Ludwig *et al.* 2000; Saganich *et al.* 2001). To test if K_V10.1 plays a role in regulation of excitability and firing of GCs, we performed whole-cell patch clamp in GCs from WT and K_V10.1 KO mice in acute cerebellar slices. The resting potential (under whole-cell current clamp) directly after breaking into the cell did not differ significantly between WT and K_V10.1 KO cells (-79.3 ± 1.5 mV, $n = 11$ and -76.0 ± 1.8 mV, $n = 5$, respectively, $P > 0.05$). Neither WT nor K_V10.1 KO cells showed spontaneous firing. Active membrane properties were evaluated by measuring the voltage response to injection of square current pulses ranging from -35 to $+35$ pA in steps of 5 pA into the soma (Fig. 2A). The resulting I - V relationship did not differ between genotypes (Fig. 2B). WT cells fired the first AP after injection of 6.4 ± 1.0 pA ($n = 11$), while K_V10.1 KO cells started firing upon injection of 5.4 ± 1.5 pA ($n = 10$, $P > 0.05$). In accordance with previous studies (D'Angelo *et al.* 1998; Chadderton *et al.* 2004; Brickley *et al.* 2007), WT and K_V10.1 KO cells displayed fast repetitive firing of APs with little or no adaptation during the depolarization (Fig. 2A). Evoked firing frequencies increased with the amplitude of the injected current (Fig. 2C). K_V10.1 channels could be implicated in the

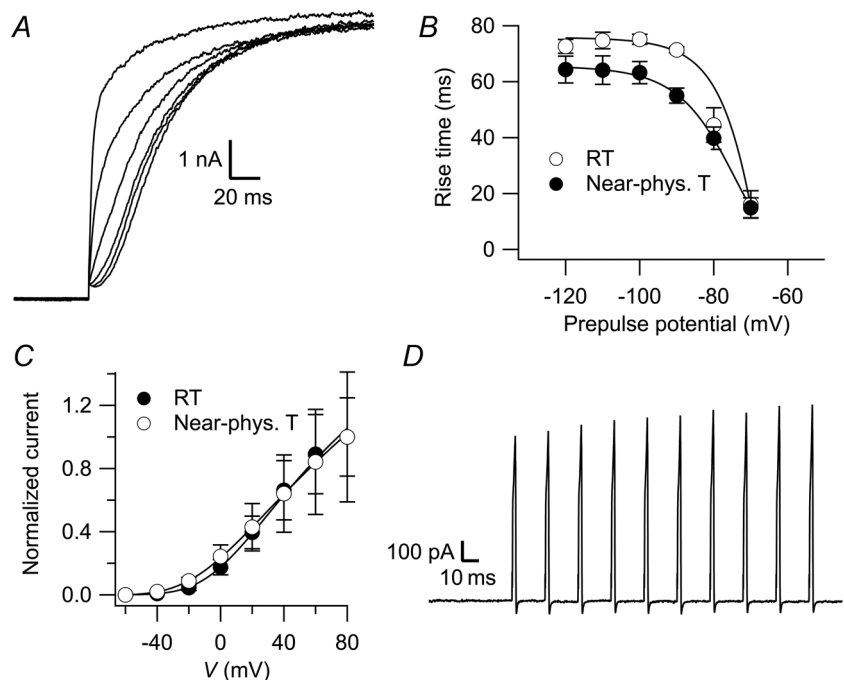
repolarization of the AP. To test this possibility, the first 8–12 APs recorded just after reaching spike threshold were averaged, and undershoot, amplitude, half-width, rise time and de-/repolarization speeds were evaluated for both WT and K_V10.1 KO. As these APs usually occurred at low frequencies, we did not expect K_V10.1 kinetics to influence the results. None of the parameters tested resulted in significant differences between genotypes (Fig. 2D–F). In summary, we detected no difference in excitability or AP properties between GCs of WT and K_V10.1 KO mice.

Kv10.1 localizes to the presynaptic terminal

In immunoelectron microscopy images on rat cerebellum using a well-characterized anti-K_V10.1 antibody (mAb62; Hemmerlein *et al.* 2006; Martin *et al.* 2008; Gómez-Varela *et al.* 2010) K_V10.1 was preferentially localized to the synapses of the parallel fibres onto the Purkinje cell spines (Fig. 3A).

To confirm presynaptic localization in the mouse, where mouse monoclonal antibodies are not optimal for morphological studies, we aimed at supporting the synaptic localization of K_V10.1 biochemically. Subcellular fractionation by centrifugation through a Ficoll gradient has been shown to be effective in separating synaptosomes from cell bodies. The presynaptic compartment can subsequently be isolated by digestion of postsynaptic proteins by trypsin treatment, as described by Boyken *et al.* (2013).

Figure 1. K_V10.1 currents at near physiological temperature in HEK-293 cells
 A, representative recording in an HEK-293 cell at near physiological temperature where a 2 s depolarization to 40 mV was preceded by 5 s prepulses ranging from -120 to -70 mV in steps of 10 mV. For clarity, only the first 200 ms are shown. The slowest trace corresponds to the -120 mV prepulse. B, 10–80% rise time of the currents measured with the protocol in A plotted against the prepulse potential at room temperature (open circles) and near physiological temperature (filled circles). C, I - V relationship as determined by measuring the whole-cell current elicited by stepping to potentials ranging from -60 to $+80$ mV in increments of 20 mV from a holding potential of -60 mV at room temperatures (open circles) and near physiological temperature (filled circles). D, currents recorded in response to a train of ten 2 ms depolarizations to 20 mV at 50 Hz.



Immunoblot analysis revealed that $K_V10.1$ was present in the synaptosome preparation and protected from proteolysis along with the presynaptic markers synaptophysin and synaptobrevin 2. The signal for $K_V10.1$ was slightly weaker after proteolysis, which might reflect some postsynaptic expression. The postsynaptic AMPA receptor was removed from the sample and was no longer detectable (Fig. 3B). This provides further evidence not only for the synaptic localization of $K_V10.1$, but specifically for a presynaptic presence of the channel, as previously suggested by Gómez-Varela *et al.* (2010) and recently confirmed by others (Chuang *et al.* 2014).

Synaptic transmission at the PF–PC synapse

The lack of evidence for an involvement of $K_V10.1$ in the regulation of the somatic membrane potential or AP firing despite the clear signal for $K_V10.1$ mRNA expression (Ludwig *et al.* 2000; Saganich *et al.* 2001; M. Kuscher, personal communication), together with electron microscopy (Gómez-Varela *et al.* 2010), light microscopy (Chuang *et al.* 2014) and the described biochemical evidence, indicates presynaptic localization of the channel. In presynaptic terminals, potassium channels determine the duration of an AP, limit frequency of APs (Matsukawa *et al.* 2003) and set the resting potential (Huang & Trussell,

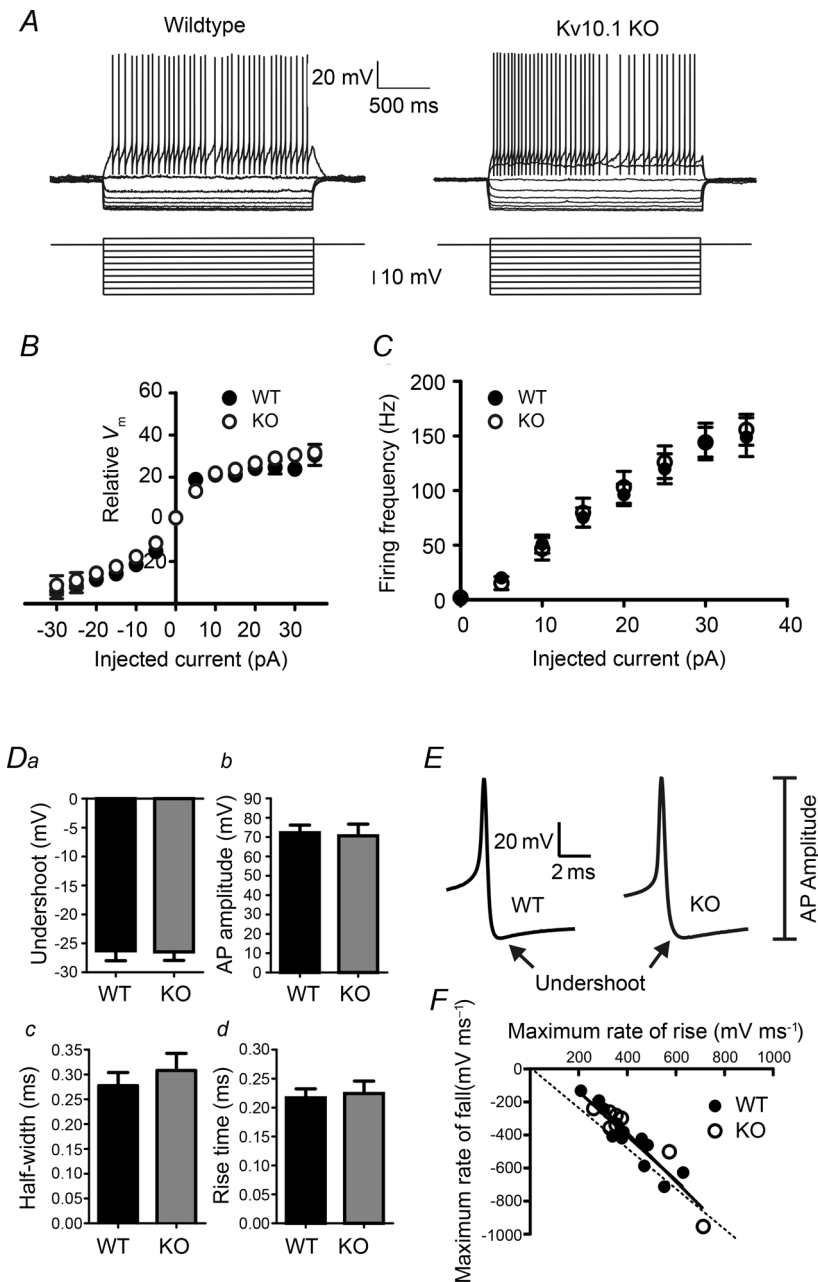


Figure 2. Somatic responses in granule cells are unaffected by deletion of $K_V10.1$

A–C, electroresponsiveness of cerebellar granule cells of WT and $K_V10.1$ KO mice. A, representative traces recorded in granule cells from WT (left) and $K_V10.1$ KO mice (right) in response to injection of square current pulses (bottom). Both genotypes showed inward rectification of the membrane potential during hyperpolarizing pulses and regular spiking after reaching a threshold potential. B, average membrane potential recorded in whole-cell current clamp mode in response to injection of square current pulses (2 s) in the presence of TTX. C, average firing frequency of WT and $K_V10.1$ KO cells upon injection of 2 s square current pulses ranging between -35 and $+35$ pA in 5 pA increments. D–F, AP properties are not altered in $K_V10.1$ KO mice. D, undershoot amplitudes measured from threshold (a), AP amplitude (b), half-width (c) and 10–90% rise time (d) are compared. Filled bars, WT, $n = 11$ cells; grey bars, $K_V10.1$ KO, $n = 8$ cells. E, representative APs recorded in a WT (left) and $K_V10.1$ KO (right) granule cell. F, maximum rate of rise of the AP plotted against the maximum rate of fall as determined by analysing the first differential. Filled circles, WT; open circles, $K_V10.1$ KO. The data points were fitted with straight lines, which were not significantly different between genotypes. The dashed line represents unity.

2011), thus controlling p_r . To evaluate basic synaptic transmission, we measured spontaneously occurring mEPSCs in Purkinje cells of WT and K_V10.1 KO mice. The inter-event interval was unchanged between WT and KO (207 ± 47 ms, $n = 8$ cells and 193 ± 57 ms, $n = 7$ cells, respectively), suggesting that the number of synapses formed onto Purkinje cells, the basal release probability and the resting Ca²⁺ levels are not affected in K_V10.1 KO mice. Furthermore, the mEPSC amplitude was unchanged (19.5 ± 1 and 18.8 ± 1.4 pA, respectively), indicating that the postsynaptic compartment is functional and unaltered in K_V10.1 KO cells.

We then recorded EPSCs in Purkinje cells evoked by extracellular stimulation of GCs (Fig. 4A, B). The kinetic parameters of EPSCs were identical in WT and K_V10.1 KO cells (Fig. 4C). Due to the variability introduced by extracellular stimulation and dendritic filtering (Roth & Häusser, 2001), no conclusion can be drawn from comparing absolute EPSC amplitudes, but the change in amplitude as a reaction to altered external Ca²⁺ concentrations can provide information about synaptic properties (Foster *et al.* 2005). Figure 4D shows the relationship between EPSC amplitude and external Ca²⁺ concentration, normalized to the amplitude at 4 mM [Ca²⁺]_o. In both genotypes, amplitude was strongly dependent on [Ca²⁺]_o and the relationship could be fitted with a sigmoid function as described previously (Mintz *et al.* 1995; Foster *et al.* 2005). Neither the normalized amplitudes nor the parameters of the fit differed significantly between WT and KO ($n = 12$

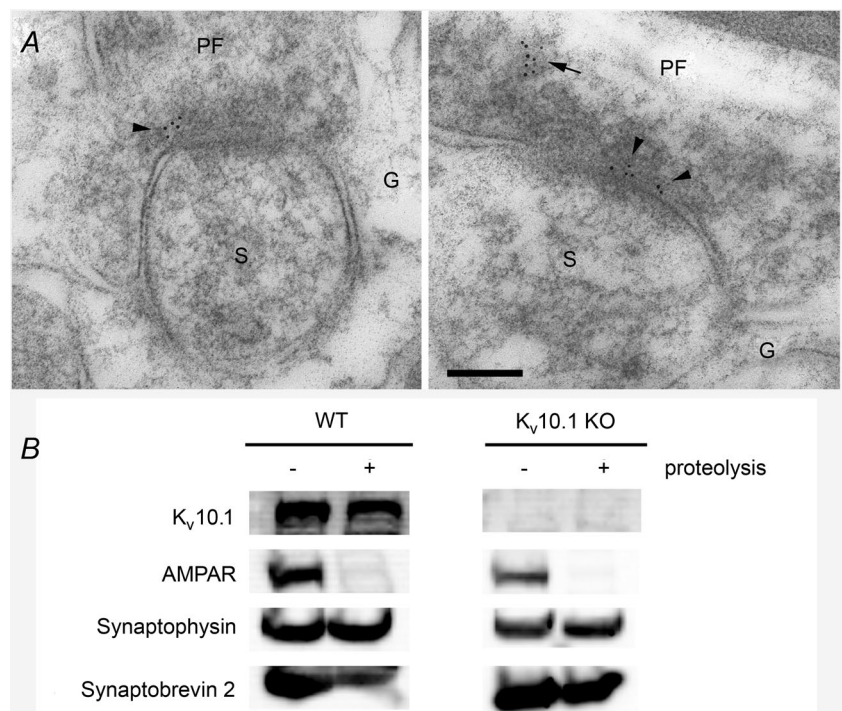
and 13 cells, respectively). To further analyse synaptic parameters, we employed a variance mean analysis (Meyer *et al.* 2001). The variance of the EPSC amplitude during repetitive, low-frequency stimulation at different [Ca²⁺]_o was plotted against the respective mean value and fitted with a parabolic function. For each cell, we determined N (64.0 ± 33.1 in WT and 44.7 ± 25.8 in KO, $P \geq 0.05$) and Q (6.96 ± 3.23 pA in WT and 8.57 ± 4.18 pA in KO, $P \geq 0.05$) values. To summarize data from various cells, the values were normalized to the maximum variance and $N \cdot Q$, the (theoretical) maximum amplitude (Valera *et al.* 2012) (Fig. 4E). As p_r is assumed to be 0.5 at the peak of the parabola, one can determine the release probability at the different Ca²⁺ concentrations. In 2 mM [Ca²⁺]_o, p_r was 0.24 ± 0.04 for the WT and 0.32 ± 0.03 for the KO ($P > 0.05$). At 0.5 mM [Ca²⁺]_o, p_r was 0.06 ± 0.01 and 0.06 ± 0.01 ; and at 4 mM p_r was 0.63 ± 0.06 and 0.69 ± 0.06 , respectively ($n = 7$ and 8, respectively, all $P > 0.05$). From these data, we conclude that the initial release probability is not significantly altered in K_V10.1 KO cells.

Two-photon Ca²⁺ imaging in the PF bouton

To address a possible increase in Ca²⁺ influx into presynaptic terminals of K_V10.1 KO cells, we performed two-photon Ca²⁺ imaging in presynaptic boutons of PFs. After loading the GC with OGB, a line scan was performed across a putative bouton (Fig. 5A, left). One to three APs

Figure 3. K_V10.1 is enriched in the presynaptic compartment

A, electron micrographs show post-embedding immunogold labelling for K_V10.1 in parallel fibre (PF) synapses on Purkinje cells spines (S) within the molecular layer of the cerebellum. Gold particles (5 nm in diameter) are localized in the presynaptic terminal close to the presynaptic plasma membrane (arrowhead) and within the cytoplasm of the PF synapse (arrow). G, Bergmann glial cells. Scale bar: 100 nm. B, immunoblot analysis of synaptosomes before and after treatment with protease reveals the presynaptic localization of K_V10.1. The protein is detected before and after trypsination, as are the presynaptic markers synaptophysin and synaptobrevin 2. The AMPA receptor is not detected after protease treatment, indicating removal of the postsynaptic part. No signal for K_V10.1 is detected in samples from K_V10.1 KO mice.



were elicited by injection of short current pulses into the soma, which led to a transient increase in fluorescence (Fig. 5B shows sample recordings in a $K_V10.1$ KO cell and a WT cell in response to three APs at 100 Hz). Single APs evoked a slight but not significantly larger increase in the Ca^{2+} response in $K_V10.1$ KO cells compared to WT (Fig. 5C). While increasing the number of APs to three nearly doubled the peak $\Delta F/F_0$ in both genotypes (Fig. 5C), an increase in frequency from 50 to 100 Hz did not cause a further rise in the WT (Fig. 5C). This is in line with earlier findings that the more intense facilitation at higher frequencies is not due to an increase in Ca^{2+} influx, for example by Ca^{2+} -dependent facilitation of Ca^{2+} currents, but by downstream mechanisms such as increase in Ca_{res} , a facilitated release machinery or saturation of endogenous Ca^{2+} buffers (Atluri & Regehr, 1996; Naraghi & Neher, 1997; Kreitzer & Regehr, 2000; Blatow *et al.* 2003; Felmy *et al.* 2003; Brenowitz & Regehr, 2007; Bornschein *et al.* 2013). In the KO, however, doubling the frequency to 100 Hz further increased the peak $\Delta F/F_0$

by 23% ($P < 0.01$). This finding is compatible with the kinetic properties of $K_V10.1$, which would take part in repolarization of the membrane depending on the frequency and pulse number (Fig. 1). Comparing the results from WT and $K_V10.1$ KO boutons, the peak $\Delta F/F_0$ after three APs at 50 Hz was increased by 31% in the KO ($P = 0.0226$, Fig. 5C) and by 73% after three APs at 100 Hz ($P = 0.0002$, Fig. 4C). This suggests frequency-dependent increases in Ca^{2+} influx during high frequency bursts of APs characteristic for GC activity (Chadderton *et al.* 2004).

Increased facilitation at the PF-PC synapse in $K_V10.1$ KO cells

We continued by investigating the consequences of loss of $K_V10.1$ on short-term modulation of synaptic strength. When tested over a range of intervals, percentage facilitation (defined as $(EPSC_3 - EPSC_1)/EPSC_1 \times 100$) decays with a time constant of 99 ms in WT and 66 ms in $K_V10.1$ KO cells (Fig. 6). Paired pulse ratio (PPR) at

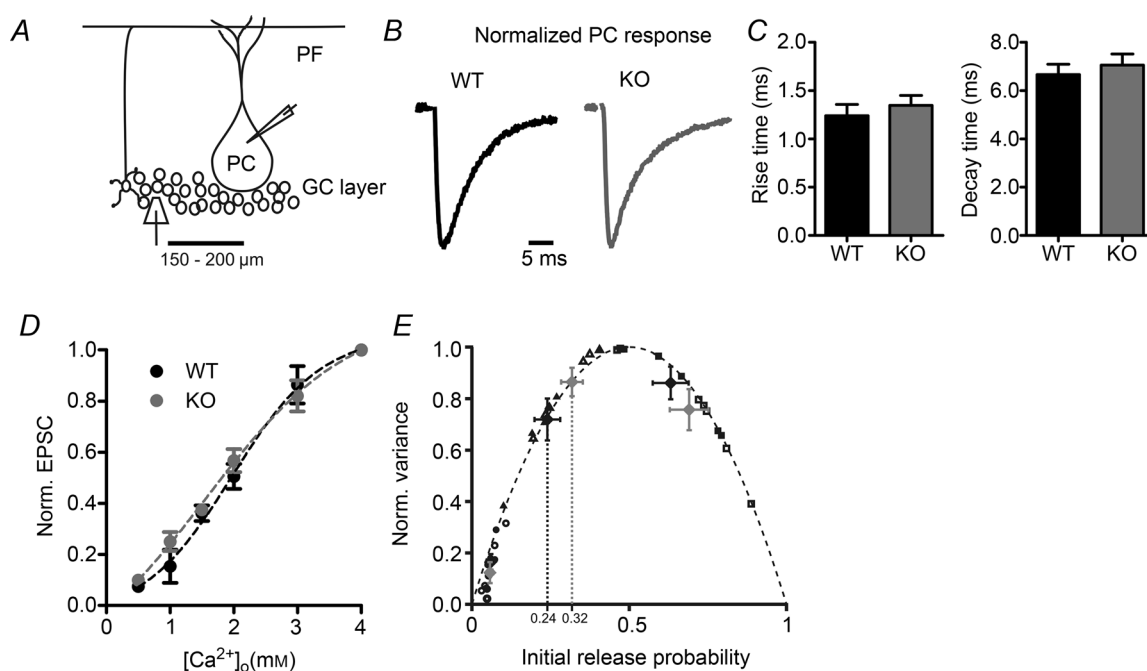


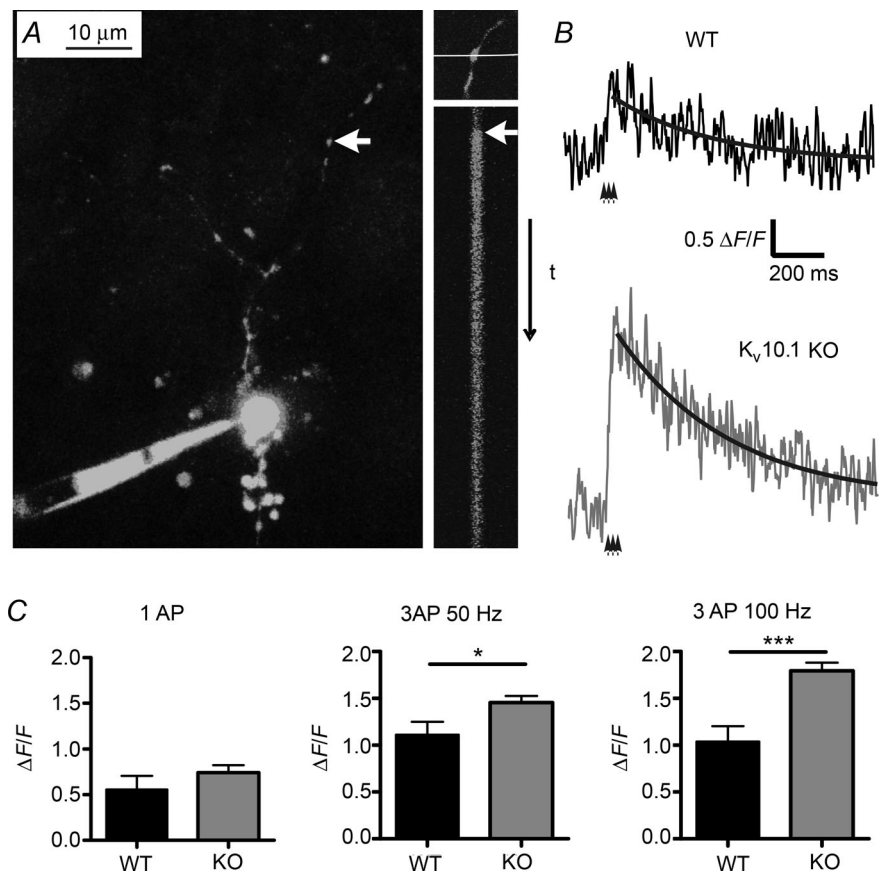
Figure 4. EPSCs in Purkinje cells evoked by extracellular stimulation

A, illustration showing the positions of the stimulation and measurement pipettes in the cerebellar cortex. PCs were whole-cell voltage clamped during extracellular stimulation in the granule layer. B, normalized sample traces in response to a single stimulus. Each trace is the average of 20 consecutive recordings. Black trace, WT; grey trace, $K_V10.1$ KO. Stimulus artefacts are blanked for clarity. C, kinetics of EPSCs in Purkinje cells. Left, 10–90% rise time of EPSC in WT (black) and $K_V10.1$ KO (grey) Purkinje cells. Right, decay time constant of EPSCs in WT (black) and $K_V10.1$ KO (grey) Purkinje cells. D, EPSC amplitudes as a function of $[Ca^{2+}]_o$. Amplitudes are normalized to the EPSC at 4 mM and fitted with a sigmoid with the formula: $base + \max/(1 + \exp(([Ca^{2+}]_{half} - [Ca^{2+}]_o)/rate))$. Parameters for WT fit were $base = -0.05$, $\max = 1.11$, $[Ca^{2+}]_{half} = 1.97$, $rate = 0.70$. Parameters for KO fit were $base = -0.31$, $\max = 1.45$, $[Ca^{2+}]_{half} = 1.57$, $rate = 1.12$. Black circles, WT, $n = 6-12$; grey circles, $K_V10.1$ KO, $n = 6-14$. E, pooled results of the variance mean analysis for all cells normalized to the maximal variance and maximal amplitude ($N \cdot Q$). Filled symbols (black, WT; grey, KO) represent initial p_r and corresponding mean variance at 0.5 mM (circles), 2 mM (triangles) and 4 mM (diamonds) $[Ca^{2+}]_o$. Open symbols are values from individual cells (black, WT, $n = 6$; grey, KO, $n = 8$).

interstimulus intervals < 50 ms was significantly increased in KO cells. Thus, the frequency-dependent increase in Ca²⁺-influx observed by Ca²⁺-imaging correlates well with a frequency-dependent increase in facilitation at the PF–PC synapse.

Examining facilitation during train stimulations (Fig. 7) revealed that the effect of K_V10.1 loss was again dependent both on the pulse number and on the stimulation frequency. In Fig. 7B–E, percentage facilitation is plotted against the stimulus number. A regular 10 Hz train evoked the same response in WT and K_V10.1 KO cells (Fig. 7B). Upon 20 Hz stimulation (Fig. 7C), the responses reached a significant difference at pulse 10 (61 ± 8%, *n* = 8 in WT and 85 ± 7%, *n* = 10 in K_V10.1 KO cells; *P* < 0.05). Stimulation with a 50 Hz train caused increased facilitation throughout the train in K_V10.1 KO cells compared to the WT (Fig. 7A, D). The difference between KO and WT cells was largest after the third pulse. During a 100 Hz train (Fig. 7E), the difference between WT and KO increased until the fifth pulse. Facilitation in both genotypes declined after reaching the peak value. To control for the number of activated fibres during a train, we measured the presynaptic volley during stimulation at the frequencies mentioned (Sabatini & Regehr, 1997) (Fig. 7F). In both genotypes, the amplitude of the volley

decreased by 15% in the second pulse, similar to the results of Kreitzer & Regehr (2000). This suggests that the number of activated fibres during the train was similar in both genotypes and no additional fibres were recruited in the KO during the train. When analysing the EPSC kinetics during the trains, it was noticeable that the 10–90% rise time of WT EPSCs did not change during a 50 Hz train, whereas it increased markedly in the K_V10.1 KO (Fig. 7G). At the tenth pulse, the KO rise time was increased 29% in comparison to the WT rise time (*n* = 20 in WT, *n* = 14 in KO, *P* < 0.05). The rise time of an EPSC is related to the duration of the Ca²⁺ transient at the release site. It has been demonstrated that AP broadening causes a prolonged duration of the active zone Ca²⁺ signal, which results in a prolonged rise time (Borst & Sakmann, 1999; Bollmann & Sakmann, 2005). The large size of the Purkinje cell complicates space clamp quality, so kinetic values have to be interpreted with care. However, the rise time could serve as a clue towards pulse number-dependent AP broadening in the K_V10.1 KO synapses. The decay time of the EPSC did not change during the train in either genotype (Fig. 7H), indicating that glutamate pooling and spillover does not contribute significantly to shaping the postsynaptic response (Takahashi *et al.* 1995). Interestingly, facilitation can be maintained during prolonged



stimulation in both genotypes (Fig. 8A). This would only be possible if the readily releasable pool (RRP) is replenished quickly (Valera *et al.* 2012), which has been shown to be Ca^{2+} -dependent (Dittman & Regehr, 1998; Dittman *et al.* 2000; Crowley *et al.* 2007). We assessed RRP replenishment by calculating the cumulative EPSC amplitude for responses normalized to the first value, fitting a line to the steady state region, and extrapolating it to the starting time (Fig. 8B) (Schneggenburger *et al.* 1999, 2002; Valera *et al.* 2012). We found the rate of vesicle replenishment in the KO to be enhanced compared to WT, which we attribute to the increased intracellular Ca^{2+} during repeated stimulation (Fig. 5). This can explain how the observed increased Ca^{2+} influx and transmitter release do not exhaust the synapse in a short time. These findings suggest that $\text{K}_V10.1$ is involved in modulation of synaptic strength during high-frequency trains. We interpret these observations as reflecting the pulse number-dependent increase in Ca^{2+} observed in the imaging experiment at the electrophysiological level.

Changes in plasticity as a result of alterations in Ca^{2+} influx and dynamics

Decreasing $[\text{Ca}^{2+}]_o$ causes less influx of Ca^{2+} into the terminal, reducing initial p_r and decelerating build-up of Ca_{res} . By influencing p_r , changes in external Ca^{2+} and Ca^{2+} influx have strong effects on the steady state amplitude of facilitation (Kreitzer & Regehr, 2000; Foster *et al.* 2005). In the WT, facilitation in 2 and 3 mM $[\text{Ca}^{2+}]_o$ reached a plateau after 3–4 pulses. Lowering $[\text{Ca}^{2+}]_o$ to 1 mM caused the facilitation in the WT to build up over 10 stimuli without reaching a stable plateau (Fig. 9A, filled circles). In $\text{K}_V10.1$ KO cells, however, facilitation in 1 mM $[\text{Ca}^{2+}]_o$ already reached a plateau after the 5th pulse (Fig. 9A, open

circles). This indicates a faster build-up of intraterminal Ca^{2+} in the $\text{K}_V10.1$ KO compared to WT. Plasticity under conditions where the release machinery (Valera *et al.* 2012) or postsynaptic receptors (Foster *et al.* 2005) are close to saturation should not differ between WT and $\text{K}_V10.1$ KO. Increasing $[\text{Ca}^{2+}]_o$ to 3 and 4 mM indeed decreased facilitation to the same extent in both genotypes (Fig. 9B). The steady state facilitations (defined as $\text{EPSC}_8/\text{EPSC}_1$) in different concentrations of $[\text{Ca}^{2+}]_o$ for WT and $\text{K}_V10.1$ KO cells are shown in Fig. 9B. In agreement with previous studies, facilitation decreased as $[\text{Ca}^{2+}]_o$ increased (Kreitzer & Regehr, 2000; Foster *et al.* 2005) and vice versa. Taken together, loss of $\text{K}_V10.1$ induced an effect only under conditions where the release machinery or the Ca^{2+} influx into the terminal is not saturated, i.e. where an increase in Ca^{2+} can translate into an increase in transmitter release.

If the increased facilitation observed in the $\text{K}_V10.1$ KO is indeed due to a faster build-up of Ca_{res} in the presynaptic terminal, removal of residual free Ca^{2+} might rescue the phenotype. Introducing EGTA into the terminal reduces residual Ca^{2+} (Adler *et al.* 1991; Atluri & Regehr, 1996). Due to its buffering properties and the very tight influx–release coupling (Schmidt *et al.* 2013), moderate concentrations of EGTA will not significantly affect the peak Ca^{2+} transient at the active zone, while the decay of residual Ca^{2+} will be accelerated. Incubation with 50 μM EGTA-AM for 15 min reduced facilitation during a 50 Hz train in both genotypes (Fig. 9C, right) and showed a different time course than under control conditions (Fig. 9C, left). However, facilitation was still enhanced in the $\text{K}_V10.1$ KO. Assuming the concentration of EGTA to be similar in terminals from both genotypes, this suggests first that more Ca^{2+} enters the terminal during each pulse and thus cannot be equally buffered by EGTA (see also Rozov *et al.* (2001), and secondly that this leads to faster build-up of residual Ca^{2+} and subsequently to enhanced facilitation even in the presence of EGTA.

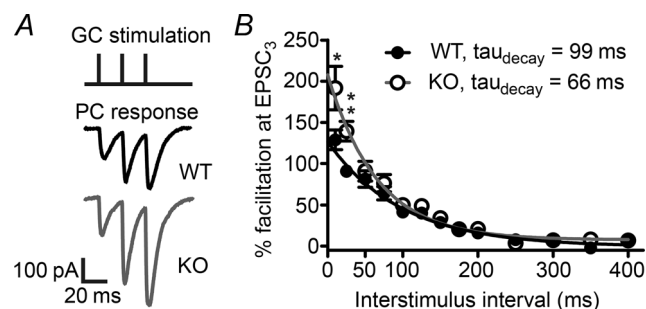


Figure 6. Increased PPR in $\text{K}_V10.1$ KO cells

A, 50 Hz stimulus train (top) with representative recordings from a WT (middle) and $\text{K}_V10.1$ KO (bottom) PC. The traces shown are the average of ten sweeps each, and stimulus artefacts have been blanked for clarity. B, facilitation of the third EPSC plotted against the interstimulus interval. The amplitude of facilitation decays exponentially with a time constant of 99 ms in the WT (filled circles) and 66 ms in the KO (open circles). Note the significant differences at intervals < 50 ms ($P \leq 0.05$, Student's t test).

Discussion

We analysed the consequences of loss of the $\text{K}_V10.1$ K^+ channel in the mouse cerebellum, providing for the first time information about the physiological function of the channel in the mammalian CNS. We found that loss of $\text{K}_V10.1$ causes increased Ca^{2+} influx into presynaptic terminals. Furthermore, enhanced facilitation was observed at PF–PC synapses of $\text{K}_V10.1$ KO mice. These effects were dependent on the stimulation frequency and number of pulses, which can be explained by the unique biophysical properties of $\text{K}_V10.1$ activation. $\text{K}_V10.1$ specifically regulates synaptic transmission at high-frequency AP trains and so acts at an intermediate

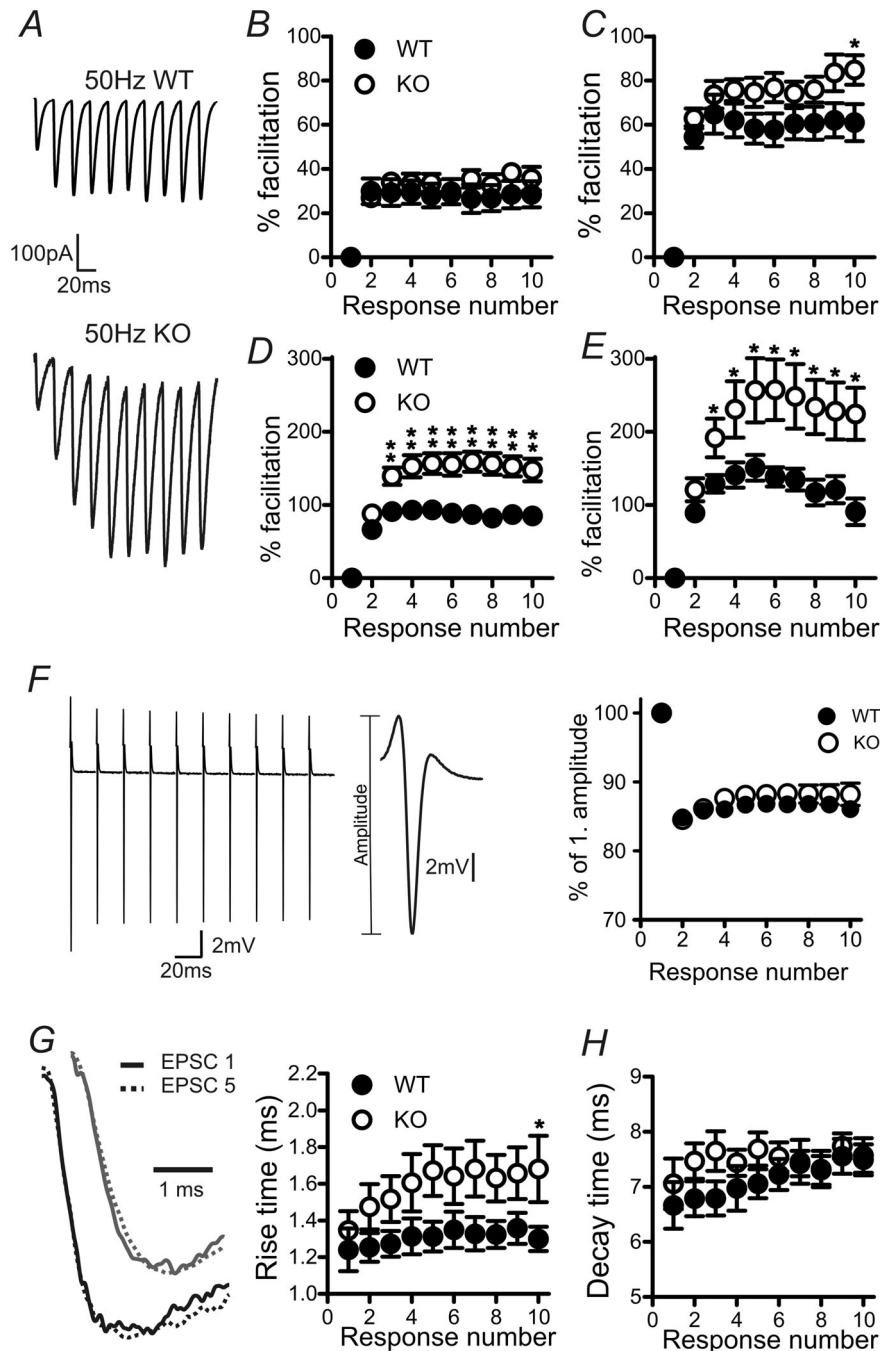
between fast high-voltage activated (HVA) and slow low-voltage activated (LVA) channels.

K_V10.1 in the CNS

Our data indicate an asymmetric distribution of K_V10.1 between soma and terminal in GCs. Despite the high signal for K_V10.1 mRNA in the GC somata (Ludwig *et al.*

2000; Saganich *et al.* 2001), no difference between WT and KO cells was found regarding excitability or AP shape at the soma (Fig. 2). This supports the described pre-synaptic localization of the channels (Gómez-Varela *et al.* 2010). Further biochemical and immunoelectron microscopy analysis showed an enrichment of K_V10.1 in the presynaptic compartment (Fig. 3; see also Chuang *et al.* 2014). By selectively targeting ion channels to subcellular

Figure 7. Facilitation of EPSCs during regular stimulus trains
 A, representative traces recorded in a WT (top) and a KO (bottom) Purkinje cell in response to a 50 Hz stimulus train. B–E, responses to train stimulations with 10 Hz (B), 20 Hz (C), 50 Hz (D) and 100 Hz (E). Percentage facilitation is defined as $(EPSC_n - EPSC_1) / EPSC_1 \times 100$ and plotted against the response number. F, left, presynaptic volley recorded in response to a 50 Hz stimulation. Stimulus artefacts have been blanked for clarity. Centre, the amplitude of the volley is a measure of the number of activated fibres. Right, relative change in the volley amplitude during a 50 Hz stimulation. The number of fibres activated during repetitive stimulation does not differ between WT and KO. G, left, representative traces of the first (continuous line) and fifth (dotted line) EPSC recorded in response to stimulation at 50 Hz in a WT (black) and K_V10.1 KO (grey) Purkinje cell. Right, 10–90% rise time of the EPSCs measured in WT (filled circles) and K_V10.1 KO (open circles) Purkinje cells during a 50 Hz stimulation plotted against the stimulus number. H, decay of the EPSCs during a 50 Hz stimulation was fitted with a single exponential and the time constant plotted against the stimulus number. In both genotypes, a slight increase in the decay time is observed, which is slightly more pronounced in the WT (filled circles) than in K_V10.1 KO cells (open circles). **P* < 0.05; ***P* < 0.01.



compartments, the cell can fine-tune the membrane properties to serve a specific purpose. In cerebellar basket cells and the calyx of Held for example, the asymmetric distribution of K_V1 and K_V3 channels ensures fast and reliable APs in the synaptic terminal, while the AP in the soma is slower and wider (Southan & Robertson, 1998; Ishikawa *et al.* 2003). The indicated presynaptic localization of $K_V10.1$ suggests a role in regulating pre-synaptic excitability and/or transmitter release.

Synaptic transmission in $K_V10.1$ KO mice

The frequency of mEPSCs was unaltered in $K_V10.1$ KO mice, suggesting that basal release probability is not affected. Furthermore, one can assume that the resting Ca^{2+} is not elevated, as this would cause an increase of spontaneous vesicle release. The kinetics of single

EPSCs were unchanged, as well as the dependence of the amplitude on the external Ca^{2+} concentration. In both genotypes, the relationship between $[Ca^{2+}]_o$ and EPSC could be fitted with a sigmoidal function. Variance mean analysis has previously been used to characterize synaptic parameters of compound EPSCs at the PF–PC synapse (Sims & Hartell, 2005; Valera *et al.* 2012). This allowed us to determine p_r at different $[Ca^{2+}]_o$ in WT and KO cells. The values were in good agreement with previous studies (Sims & Hartell, 2005; Valera *et al.* 2012; Schmidt *et al.* 2013), and suggest that the initial p_r is not altered in $K_V10.1$ KO cells. These results indicate that $K_V10.1$ channels do not participate significantly in repolarizing the first AP of a train as the resulting changes in AP shape should have altered p_r . As we observe an increase in $K_V10.1$ -mediated current amplitude in HEK cells upon repeated stimulation at 50 Hz, we think this indicates that the $K_V10.1$ channel only becomes active later in a train of APs (see below).

The average mEPSC amplitude was more than twice the quantal size yielded by variance mean analysis in both genotypes. However, one has to consider that mEPSCs from climbing fibre synapses will be included, as they cannot be distinguished from events originating in parallel fibres. Furthermore, only mEPSCs larger than a certain detection limit (~ 10 pA) were measured. Small events, especially from distal parts of the dendritic arbour, can be lost in dendritic filtering and noise. Thus, our recordings systematically overestimated mEPSC amplitude.

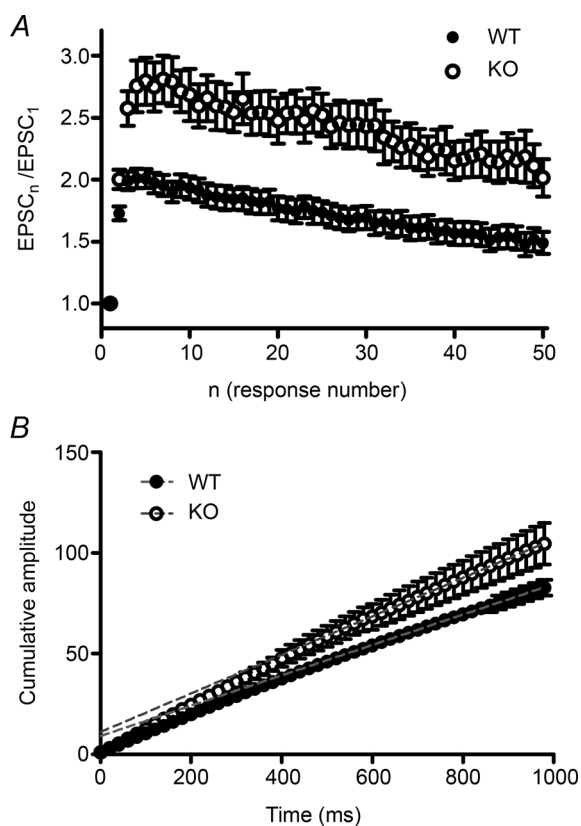


Figure 8. Facilitation during prolonged stimulation

A, normalized EPSC amplitude ($EPSC_n/EPSC_1$) during 50 Hz stimulation at the PF–PC synapse plotted against response number. Facilitation decays only slowly in both genotypes (filled circles, WT; open circles, KO). B, cumulative plot of normalized EPSC amplitudes shown in A. A line is fitted to the steady-state region of the plot (dotted red line, WT; dotted blue line, KO) and extrapolated to intercept the y-axis at time 0. The slope represents the relative replenishment rate of the RRP (Schneggenburger *et al.*, 1999, 2002). The fitting function is $0.076t + 9.06$ for the WT, and $0.096t + 11.06$ for the $K_V10.1$. filled circles, WT ($n = 24$); open circles, KO ($n = 19$).

Increased Ca^{2+} influx and facilitation in the absence of $K_V10.1$

Interestingly, stimulation with a short burst of APs increased the Ca^{2+} influx to a greater extent in the KO than in the WT. This effect was stronger at 100 Hz than at 50 Hz (Fig. 5). The frequency- (and pulse number-) dependent increase in Ca^{2+} influx resulted in enhanced facilitation of the PF–PC synapse in the $K_V10.1$ KO at input frequencies > 20 Hz, whose extent and time course was also frequency-dependent (Fig. 7). We can exclude significant additional fibre recruitment in the KO as the fibre volley amplitude was unchanged between WT and KO (see also Valera *et al.* 2012). We did not detect a broadening in the field potential recording corresponding to the increase in EPSC rise time (Fig. 7G), probably because the extracellular recording failed to resolve this quite small difference.

It is intriguing how efficiently the PF synapse can increase its output without depleting the RRP. This property indicates a constant, rapid replenishment of the RRP, which is a Ca^{2+} -dependent process (Dittman & Regehr, 1998; Dittman *et al.* 2000; Crowley *et al.* 2007). We found increased RRP replenishment in the KO, which

can explain that facilitation decays only slowly even during prolonged stimulation, with the KO values constantly well above the WT (Fig. 8). Previous studies have shown medium, heterogeneous p_r at PF synapses (Valera *et al.* 2012; Schmidt *et al.* 2013). Valera *et al.* (2012) suggested that during tract stimulation high p_r synapses respond to the first stimulus in a train whereas low p_r synapses become subsequently recruited as intracellular Ca²⁺ rises. Our data support this notion, as the increased Ca²⁺ influx into KO synapses could promote the recruitment of low p_r synapses during trains, further contributing to the activity-dependent increase in EPSC size. Even though a single synapse could suffer from rundown caused by increased transmitter release, the compound response would remain or increase in size as new synapses become recruited.

The finding that the rise time of the EPSC during a 50 Hz train also increased in the KO, but remained constant in the WT, corroborates our hypothesis of a use-dependent AP broadening in the KO, as AP shape, the time course of Ca²⁺ influx and EPSC rise time are tightly related (Borst & Sakmann, 1999; Bollmann & Sakmann, 2005). Our results

are reminiscent of the use-dependent AP broadening observed in the hippocampal mossy fibre bouton. There, cumulative inactivation of K_V1 channels during trains of stimuli causes a broadening of the presynaptic AP and subsequently facilitation of EPSCs (Geiger & Jonas, 2000; Alle *et al.* 2011). Use-dependent increase in Ca²⁺ influx has not been shown at the PF–PC synapse (Kreitzer & Regehr, 2000), indicating that either channels taking part in repolarization of the AP at this synapse do not inactivate or that cumulative inactivation is compensated for by other channels. To our knowledge, no functional study has been done on K_V1 channels in PF–PC synapses, but mRNA for K_V1.1, 1.3 and 1.5 was detected in GCs. Of these, K_V1.3 shows cumulative inactivation, and, in the presence of regulatory subunits, also K_V1.1 and 1.5 can show inactivation (Mathie *et al.* 2003). During repeated activity of the synapse, these channels will suffer increasing inactivation, while the depolarizations will accelerate the activation kinetics of K_V10.1 (Fig. 1), allowing it to participate in AP repolarization specifically at trains of high-frequency activity and to ensure a constant AP waveform (Sabatini & Regehr, 1997) during the AP train.

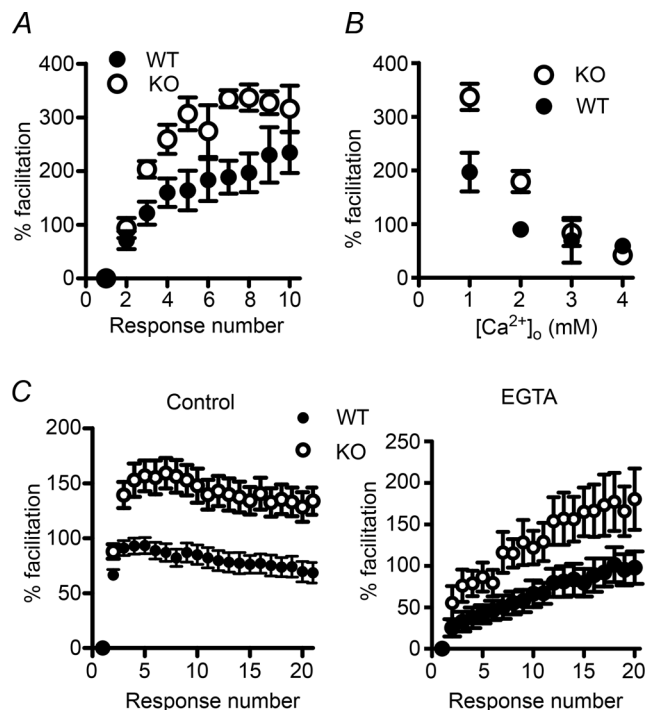


Figure 9. The effects of altering extracellular or intracellular calcium on facilitation at the PF–PC synapse

A, response to 50 Hz train stimulation in 1 mM external Ca²⁺. B, percentage facilitation at the 8th EPSC of a 50 Hz train, when facilitation reached a plateau. Open circles, K_V10.1 KO; filled circles, WT. Each data point is the average of 5–10 cells. C, response to a 50 Hz stimulus under control conditions (left) and after incubation with 50 μM EGTA-AM (right). Both amplitude and time course are changed after incubation with EGTA-AM. Facilitation in the KO (open circles) was increased and rose faster than in the WT (filled circles).

Physiological implications of K_V10.1 loss

The behavioural consequences of K_V10.1 deletion are mild; KO mice show only slightly increased spontaneous locomotor activity and an increased sensitivity to Haloperidol-induced catalepsy, both of which have been related to alterations in neurotransmitter systems (Ufartes *et al.* 2013). Knock-down of K_V10.1 in zebrafish has been shown to severely disrupt development of the CNS (Stengel *et al.* 2012). Note that comparing knock-down and knock-out approaches is not always straightforward, as has been shown recently by Yang *et al.* (2013). There, the phenotypes observed upon knocking down or knocking out the synaptic protein complex were quite different, depending on the method employed.

The role of K_V10.1 in mammalian development is unlikely to be as important as in zebrafish. K_V10.1 expression starts after birth, and reaches a maximum only in adult animals. K_V10.1 KO mice breed and develop normally, and show no micro- or macroanatomical abnormalities. No compensatory up-regulation of other ion channel genes could be detected in KO mice (Ufartes *et al.* 2013), and our mEPSC data further speak against alterations in synapse number or postsynaptic organization.

Our data assign a new role to K_V10.1, different from both HVA and LVA channels. It acts as a specific regulator of high-frequency AP trains and prevents excessive neurotransmitter release from saturating and in the end even depleting the synapse and endanger faithful encoding of signals from GCs to Purkinje cells.

References

- Adler E, Augustine G, Duffy S & Charlton M (1991). Alien intracellular calcium chelators attenuate neurotransmitter release at the squid giant synapse. *J Neurosci* **11**, 1496–1507.
- Alle H, Kubota H & Geiger JRP (2011). Sparse but highly efficient Kv3 outpace BKCa channels in action potential repolarization at hippocampal mossy fiber boutons. *J Neurosci* **31**, 8001–8012.
- Atluri PP & Regehr WG (1996). Determinants of the time course of facilitation at the granule cell to Purkinje cell synapse. *J Neurosci* **16**, 5661–5671.
- Bao J, Reim K & Sakaba T (2010). Target-dependent feedforward inhibition mediated by short-term synaptic plasticity in the cerebellum. *J Neurosci* **30**, 8171–8179.
- Blatow M, Caputi A, Burnashev N, Monyer H & Rozov A (2003). Ca²⁺ buffer saturation underlies paired pulse facilitation in calbindin-D28k-containing terminals. *Neuron* **38**, 79–88.
- Bollmann JH & Sakmann B (2005). Control of synaptic strength and timing by the release-site Ca²⁺ signal. *Nat Neurosci* **8**, 426–434.
- Bornschein G, Arendt O, Hallermann S, Brachtendorf S, Eilers J & Schmidt H (2013). Paired-pulse facilitation at recurrent Purkinje neuron synapses is independent of calbindin and parvalbumin during high-frequency activation. *J Physiol* **591**, 3355–3370.
- Borst JGG & Sakmann B (1999). Effect of changes in action potential shape on calcium currents and transmitter release in a calyx-type synapse of the rat auditory brainstem. *Phil Trans R Soc B* **354**, 347–355.
- Boyken J, Grønberg M, Riedel D, Urlaub H, Jahn R & Chua JJ (2013). Molecular profiling of synaptic vesicle docking sites reveals novel proteins but few differences between glutamatergic and GABAergic synapses. *Neuron* **78**, 285–297.
- Brenowitz SD & Regehr WG (2007). Reliability and heterogeneity of calcium signaling at single presynaptic boutons of cerebellar granule cells. *J Neurosci* **27**, 7888–7898.
- Brickley SG, Aller MI, Sandu C, Veale EL, Alder FG, Sambhi H, Mathie A & Wisden W (2007). TASK-3 two-pore domain potassium channels enable sustained high-frequency firing in cerebellar granule neurons. *J Neurosci* **27**, 9329–9340.
- Chadderton P, Margrie TW & Hausser M (2004). Integration of quanta in cerebellar granule cells during sensory processing. *Nature* **428**, 856–860.
- Chen Y, Sánchez A, Rubio ME, Kohl T, Pardo LA & Stühmer W (2011). Functional K_v10.1 channels localize to the inner nuclear membrane. *PLoS ONE* **6**, e19257.
- Chuang C-C, Jow G-M, Lin H-M, Weng Y-H, Hu J-H, Peng Y-J, Chiu Y-C, Chiu M-M & Jeng C-J (2014). The punctate localization of rat Eag1 K⁺ channels is conferred by the proximal post-CNBHD region. *BMC Neuroscience* **15**, 23.
- Clements JD & Silver RA (2000). Unveiling synaptic plasticity: a new graphical and analytical approach. *Trends Neurosci* **23**, 105–113.
- Crowley JJ, Carter AG & Regehr WG (2007). Fast vesicle replenishment and rapid recovery from desensitization at a single synaptic release site. *J Neurosci* **27**, 5448–5460.
- D'Angelo E, Filippi GD, Rossi P & Taglietti V (1998). Ionic mechanism of electroresponsiveness in cerebellar granule cells implicates the action of a persistent sodium current. *J Neurophysiol* **80**, 493–503.
- Dittman JS, Kreitzer AC & Regehr WG (2000). Interplay between facilitation, depression, and residual calcium at three presynaptic terminals. *J Neurosci* **20**, 1374–1385.
- Dittman JS & Regehr WG (1998). Calcium dependence and recovery kinetics of presynaptic depression at the climbing fiber to Purkinje cell synapse. *J Neurosci* **18**, 6147–6162.
- Douyard J, Shen L, Huganir RL & Rubio ME (2007). Differential neuronal and glial expression of GluR1 AMPA receptor subunit and the scaffolding proteins SAP97 and 4.1 N during rat cerebellar development. *J Comp Neurol* **502**, 141–156.
- Felmy F, Neher E & Schneggenburger R (2003). Probing the intracellular calcium sensitivity of transmitter release during synaptic facilitation. *Neuron* **37**, 801–811.
- Fischer von Mollard G, Südhof TC & Jahn R (1991). A small GTP-binding protein dissociates from synaptic vesicles during exocytosis. *Nature* **349**, 79–81.
- Foster KA, Crowley JJ & Regehr WG (2005). The influence of multivesicular release and postsynaptic receptor saturation on transmission at granule cell to Purkinje cell synapses. *J Neurosci* **25**, 11655–11665.
- García-Ferreiro RE, Kerschensteiner D, Major F, Monje F, Stühmer W & Pardo LA (2004). Mechanism of block of hEag1 K⁺ channels by imipramine and astemizole. *J Gen Physiol* **124**, 301–317.
- Geiger JRP & Jonas P (2000). Dynamic control of presynaptic Ca²⁺ inflow by fast-inactivating K⁺ channels in hippocampal mossy fiber boutons. *Neuron* **28**, 927–939.
- Gómez-Varela D, Kohl T, Schmidt M, Rubio ME, Kawabe H, Nehring RB, Schäfer S, Stühmer W & Pardo LA (2010). Characterization of Eag1 channel lateral mobility in rat hippocampal cultures by single-particle-tracking with quantum dots. *PLoS ONE* **5**, e8858.
- Hemmerlein B, Weseloh RM, Mello de Queiroz F, Knotgen H, Sanchez A, Rubio ME, Martin S, Schliephacke T, Jenke M, Heinz Joachim R, Stuhmer W & Pardo LA (2006). Overexpression of Eag1 potassium channels in clinical tumours. *Mol Cancer* **5**, 41.
- Huang H & Trussell LO (2011). KCNQ5 channels control resting properties and release probability of a synapse. *Nat Neurosci* **14**, 840–847.
- Humeau Y, Doussau F, Popoff MR, Benfenati F & Poulain B (2007). Fast changes in the functional status of release sites during short-term plasticity: involvement of a frequency-dependent bypass of Rac at Aplysia synapses. *J Physiol* **583**, 983–1004.
- Humeau Y, Popoff MR, Kojima H, Doussau F & Poulain B (2002). Rac GTPase plays an essential role in exocytosis by controlling the fusion competence of release sites. *J Neurosci* **22**, 7968–7981.
- Humeau Y, Vitale N, Chasserot-Golaz S, Dupont J-L, Du G, Frohman MA, Bader M-F & Poulain B (2001). A role for

- phospholipase D1 in neurotransmitter release. *Proc Natl Acad Sci USA* **98**, 15300–15305.
- Ishikawa T, Nakamura Y, Saitoh N, Li W-B, Iwasaki S & Takahashi T (2003). Distinct roles of K_v1 and K_v3 potassium channels at the calyx of Held presynaptic terminal. *J Neurosci* **23**, 10445–10453.
- Isope P & Barbour B (2002). Properties of unitary granule cell→Purkinje cell synapses in adult rat cerebellar slices. *J Neurosci* **22**, 9668–9678.
- Konnerth A, Llano I & Armstrong CM (1990). Synaptic currents in cerebellar Purkinje cells. *Proc Natl Acad Sci USA* **87**, 2662–2665.
- Kreitzer AC & Regehr WG (2000). Modulation of transmission during trains at a cerebellar synapse. *J Neurosci* **20**, 1348–1357.
- Ludwig J, Terlau H, Wunder F, Brüggemann A, Pardo LA, Marquardt A, Stühmer W & Pongs O (1994). Functional expression of a rat homologue of the voltage gated ether *à* go-go potassium channel reveals differences in selectivity and activation kinetics between the Drosophila channel and its mammalian counterpart. *EMBO J* **13**, 4451–4458.
- Ludwig J, Weseloh R, Karschin C, Liu Q, Netzer R, Engeland B, Stansfeld C & Pongs O (2000). Cloning and functional expression of rat eag2, a new member of the *Ether-à-go-go* family of potassium channels and comparison of its distribution with that of eag1. *Mol Cell Neurosci* **16**, 59–70.
- Martin S, Lino de Oliveira C, Mello de Queiroz F, Pardo LA, Stühmer W & Del Bel E (2008). Eag1 potassium channel immunohistochemistry in the CNS of adult rat and selected regions of human brain. *Neuroscience* **155**, 833–844.
- Mathie A, Clarke C, Ranatunga K & Veale E (2003). What are the roles of the many different types of potassium channel expressed in cerebellar granule cells? *Cerebellum* **2**, 11–25.
- Matsukawa H, Wolf AM, Matsushita S, Joho RH & Knöpfel T (2003). Motor dysfunction and altered synaptic transmission at the parallel fiber-Purkinje cell synapse in mice lacking potassium channels K_v3.1 and K_v3.3. *J Neurosci* **23**, 7677–7684.
- Meyer AC, Neher E & Schneggenburger R (2001). Estimation of quantal size and number of functional active zones at the calyx of held synapse by nonstationary EPSC variance analysis. *J Neurosci* **21**, 7889–7900.
- Mintz IM, Sabatini BL & Regehr WG (1995). Calcium control of transmitter release at a cerebellar synapse. *Neuron* **15**, 675–688.
- Naraghi M & Neher E (1997). Linearized buffered Ca²⁺ diffusion in microdomains and its implications for calculation of [Ca²⁺] at the mouth of a calcium channel. *J Neurosci* **17**, 6961–6973.
- Reid CA & Clements JD (1999). Postsynaptic expression of long-term potentiation in the rat dentate gyrus demonstrated by variance-mean analysis. *J Physiol* **518**, 121–130.
- Roth A & Häusser M (2001). Compartmental models of rat cerebellar Purkinje cells based on simultaneous somatic and dendritic patch-clamp recordings. *J Physiol* **535**, 445–472.
- Rozov A, Burnashev N, Sakmann B & Neher E (2001). Transmitter release modulation by intracellular Ca²⁺ buffers in facilitating and depressing nerve terminals of pyramidal cells in layer 2/3 of the rat neocortex indicates a target cell-specific difference in presynaptic calcium dynamics. *J Physiol* **531**, 807–826.
- Sabatini BL & Regehr WG (1997). Control of neurotransmitter release by presynaptic waveform at the granule cell to Purkinje cell synapse. *J Neurosci* **17**, 3425–3435.
- Saganich MJ, Machado E & Rudy B (2001). Differential expression of genes encoding subthreshold-operating voltage-gated K⁺ channels in brain. *J Neurosci* **21**, 4609–4624.
- Schmidt H, Brachtendorf S, Arendt O, Hallermann S, Ishiyama S, Bornschein G, Gall D, Schiffmann SN, Heckmann M & Eilers J (2013). Nanodomain coupling at an excitatory cortical synapse. *Curr Biol* **23**, 244–249.
- Schneggenburger R, Meyer AC & Neher E (1999). Released fraction and total size of a pool of immediately available transmitter quanta at a calyx synapse. *Neuron* **23**, 399–409.
- Schneggenburger R, Sakaba T & Neher E (2002). Vesicle pools and short-term synaptic depression: lessons from a large synapse. *Trends Neurosci* **25**, 206–212.
- Silver RA (2003). Estimation of nonuniform quantal parameters with multiple-probability fluctuation analysis: theory, application and limitations. *J Neurosci Meth* **130**, 127–141.
- Silver RA, Momiyama A & Cull-Candy SG (1998). Locus of frequency-dependent depression identified with multiple-probability fluctuation analysis at rat climbing fibre-Purkinje cell synapses. *J Physiol* **510**, 881–902.
- Sims RE & Hartell NA (2005). Differences in transmission properties and susceptibility to long-term depression reveal functional specialization of ascending axon and parallel fiber synapses to Purkinje cells. *J Neurosci* **25**, 3246–3257.
- Southan AP & Robertson B (1998). Patch-clamp recordings from cerebellar basket cell bodies and their presynaptic terminals reveal an asymmetric distribution of voltage-gated potassium channels. *J Neurosci* **18**, 948–955.
- Stengel R, Rivera-Milla E, Sahoo N, Ebert C, Bollig F, Heinemann SH, Schonherr R & Englert C (2012). Kcnh1 voltage-gated potassium channels are essential for early zebrafish development. *J Biol Chem* **287**, 35565–35575.
- Takahashi M, Kovalchuk Y & Attwell D (1995). Pre- and postsynaptic determinants of EPSC waveform at cerebellar climbing fiber and parallel fiber to Purkinje cell synapses. *J Neurosci* **15**, 5693–5702.
- Terlau H, Ludwig J, Steffan R, Pongs O, Stühmer W & Heinemann S (1996). Extracellular Mg²⁺ regulates activation of rat eag potassium channel. *Pflugers Arch* **432**, 301–312.
- Ufartes R, Schneider T, Mortensen LS, de Juan Romero C, Hentrich K, Knoetgen H, Beilinson V, Moebius W, Tarabykin V, Alves F, Pardo LA, Rawlins JNP & Stuehmer W (2013). Behavioural and functional characterization of Kv10.1 (Eag1) knockout mice. *Hum Mol Genet* **22**, 2247–2262.

- Valera AM, Doussau F, Poulain B, Barbour B & Isope P (2012). Adaptation of granule cell to Purkinje cell synapses to high-frequency transmission. *J Neurosci* **32**, 3267–3280.
- Warmke JW & Ganetzky B (1994). A family of potassium channel genes related to eag in *Drosophila* and mammals. *Proc Natl Acad Sci USA* **91**, 3438–3442.
- Wheeler D, Randall A & Tsien R (1996). Changes in action potential duration alter reliance of excitatory synaptic transmission on multiple types of Ca²⁺ channels in rat hippocampus. *J Neurosci* **16**, 2226–2237.
- Wu CF, Ganetzky B, Haugland FN & Liu AX (1983). Potassium currents in *Drosophila*: different components affected by mutations of two genes. *Science* **220**, 1076–1078.
- Yang X, Cao P & Südhof TC (2013). Deconstructing complexin function in activating and clamping Ca²⁺-triggered exocytosis by comparing knockout and knockdown phenotypes. *Proc Natl Acad Sci USA* **110**, 20777–20782.
- Zucker RS & Regehr WG (2002). Short-term synaptic plasticity. *Annu Rev Physiol* **64**, 355–405.

Additional information

Competing interest

The authors declare no competing financial interests.

Author contributions

L.S.M., T.S., H.S., J.E., W.S. and L.A.P. designed experiments. L.S.M., Z.F., M.E.R., H.S. and L.A.P. performed experiments. L.S.M., Z.F., H.S. and L.A.P. analysed data. L.S.M., H.S., J.E., A.B.F. and R.U. contributed analytical or experimental tools. L.S.M. wrote the manuscript with critical inputs from H.S., T.S., Z.F., A.B.F., R.U., J.E., W.S. and L.A.P. All authors

approved the final version of the manuscript. The experiments were performed at the Max-Planck-Institute of Experimental Medicine, Göttingen, the Max-Planck-Institute of Biophysical Chemistry, Göttingen, and the Carl-Ludwig-Institute of Physiology, Leipzig.

Funding

This work was supported by an IMPRS fellowship to L.S.M., a GGNB Excellence Stipend to A.B.F., NIH grant 1R01DC013048-01 to M.E.R., the Japanese Society for the Promotion of Science, Core-to-Core Program A, Advance Research Networks to T.S., and DFG grant EI 342/4-1 to J.E. and H.S.

Acknowledgements

We thank G. Bethge, B. Heidrich, S. Schmidt and H. Widera for expert technical assistance.

Authors' present addresses

Z. Farsi, Max Planck Institute for Biophysical Chemistry, 37077 Göttingen, Germany.

A. Barrantes-Freer, Department of Neuropathology, University Medical Center Göttingen, 37099 Göttingen, Germany.

M. E. Rubio, Department of Otolaryngology and Neurobiology, University of Pittsburgh Medical School, Pittsburgh, PA 15261, USA.

T. Sakaba, Doshisha University, Kyoto 619-0225, Japan.